Electrostatic Spinning of Acrylic Microfibers

PETER K. BAUMGARTEN[1]

E. I. du Pont de Nemours & Co., Engineering Technology Laboratory, Wilmington, Delaware

Received July 20, 1970; accepted January 8, 1971

Fibers measuring less than 1 μ in diameter were spun by electrostatic means from dimethyl formamide (DMF) solutions of acrylic resin. High-speed photographs showed that a single fiber was drawn out from the electrically charged drop which was suspended from a metal capillary. Calculations indicated that spinning velocity probably reached and perhaps exceeded the velocity of sound in air. Electric field maps and other theoretical considerations showed that electric conductivity plays an important role in the spinning mechanism. The effects on fiber diameter and jet length of solution viscosity, surrounding gas, flow rate, voltage, and geometry were determined.

INTRODUCTION

When an electric potential is applied to a liquid drop hanging from a metal tube, the drop elongates, forms a tip, and from the tip fine droplets or very fine fibers are dispersed. The phenomenon of electrostatic droplet formation has been discussed in the literature (1–3). To generate fibers or a filament, a solution of a fiber-forming polymer is necessary. The patent literature of the 30's and 40's contains references to the electrostatic spinning of acetate rayon (4, 5). Experiments in this laboratory showed that other polymers might also be spun electrically from solution, and that in particular dimethyl formamide solutions of a modified polyacrylonitrile could readily be made to generate microfibers with diameters in the range of 0.05 to 1.1 μ. Since the factors surrounding the spinning process were not well known, a study was made to analyze it from an experimental and theoretical standpoint. The work was concentrated on the acrylic resin-DMF system.

[1] Present address: E. I. du Pont de Nemours & Company, Explosives Department, Gibbstown, New Jersey 08027.

EXPERIMENTAL

Most of the experimental work was carried out with the apparatus shown in Fig. 1. The spinning drop was suspended from a stainless steel capillary tube, and maintained constant in size by adjusting the feed rate of an infusion (positive displacement) pump. A dc high-voltage supply was connected to the capillary tube, and the fibers were collected on a grounded metal screen. For the photographic study, an Edgerton, Germeshauser, and Grier Model 549 electronic flash, a Fresnel lens, and a 4 × 5 in. view camera with 90-mm lens were placed in line with the spinning fiber. A small black paper disk was cemented on the Fresnel lens to serve as background for the illuminated fiber. The EG & G microflash with a flash duration of about 0.8×10^{-6} sec was able to stop the action completely. "Fastax" motion pictures at 4000 to 5000 frames/sec were taken with a similar setup using synchronized electronic flash. To allow changing the spinning atmosphere, a plastic shroud could be set up to surround the capillary and screen. The power supply was a 30,000-V, 1.8-mA Universal Voltronics unit. Current was read on a 100-μA meter. The acrylic resin was a com-

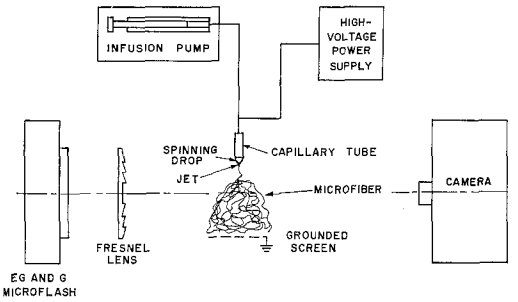

FIG. 1. Experimental setup for photographic study.

mercial copolymer of 93.6% acrylonitrile, 6% methyl acrylate, and 0.4% sodium styrene sulfonate with an intrinsic viscosity of 1.5. Electron photomicrographs at 2800 to 11,600X magnification were taken of the fibers produced, and a mean fiber diameter was obtained by averaging the diameters of 25 lengths appearing in the photographs.

RESULTS

Microflash Photographs and Effect of Solution Viscosity. Figures 2*A* and 2*B* show a typical series of microflash photographs of acrylic resin-dimethyl formamide solutions differing in concentration and viscosity. With pure DMF, fine droplets were formed. Fiber formation started with a 7.5 wt % solution (1.7 poise) and continued to 20 wt % (215 poise). With 17.5 and 20 wt %, however, drying of the fiber was incomplete, and the fiber began to stick to itself in mid-air. Note that as viscosity increased, the spinning drop changed from approximately hemispherical to conical. The length of the jet increased, as shown also in Fig. 3. The jet length was measured from the tip of the spinning drop to the onset of waves in the fiber. Fiber diameter also increased with solution viscosity as shown in Fig. 3 and was approximately proportional to jet length.

Electron photomicrographs showed the collected dry fiber to have the appearance of smooth, straight cylinders. In any one photomicrograph, fiber lengths varied in diameter about twofold. Fiber ends were hardly ever found in the photomicrographs, corroborating the conclusion drawn from the flash pictures that electrostatic spinning of the polyacrylonitrile solutions studied here produced a single continuous fiber. Little droplets, or spatter, were occasionally noted in the pictures.

Spinning under "normal" conditions, such as shown in the first frame of Fig. 2*B*, was investigated further using "Fastax" motion pictures at 4560 frames/sec with synchronized flash. The pictures revealed that fiber loops shot out radially from the jet at a velocity of 6 to 7 m/sec and then fell toward the screen at 1.8 to 3.7 m/sec. The motion of the waves just below the spinning jet was irregular, no corkscrew motion being apparent. The frame speed of the movies was not high enough to determine the velocity of the very first small waves.

Solids Content of Fibers. The solids content of the acrylic fibers at laydown was determined by the weight loss in a 60°C vacuum oven. Table I gives the results. These data and the dry fiber diameter data obtained from the photomicrographs allow estimation of fiber velocity and diameter.

Effect of Flow Rate, Voltage, and Gap. Figure 4 shows fiber diameter and jet length *vs.* solution feed rate for 12.5% solution at constant voltage and gap. The range of spinnable feed rates was about tenfold, with periodic disappearance of the spinning drop marking the low end of the range, and occasional spatter marking the top end. Effect on fiber diameter was small. Jet length approximately doubled. The midpoint of the spinnable range could be termed as optimum. When voltage was increased, this optimum feed rate increased as shown in Fig. 5. Effect of voltage and spinneret-to-ground spacing ("gap") at the optimum spinning rate is shown in Figs. 6 and 7. Jet length increased with increased voltage and reduced gap. Fiber diameter went through a minimum with increasing voltage at a 50-mm gap, but not clearly so at a 75-mm gap.

The data shown in Figs. 3 to 7 were obtained with a positively charged 1.5 mm

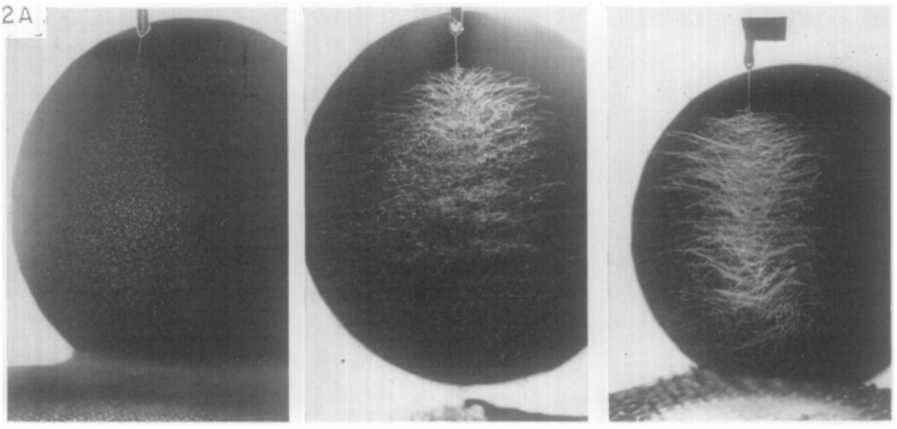

FIG. 2A. Microflash photographs of electrostatic spinning. 10,000 V + direct current. Spinneret to ground spacing 50 mm. Solution feed rate 0.028 to 0.035 cc/min.

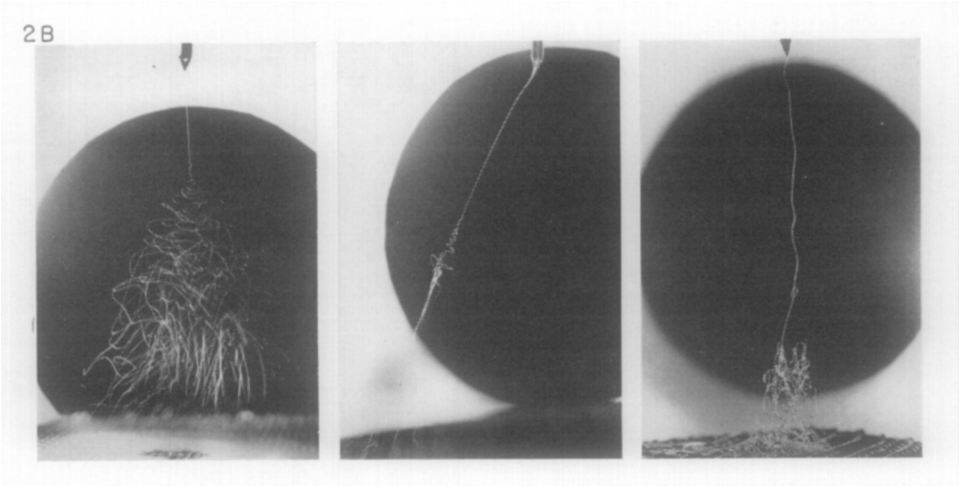

FIG. 2B. Microflash photographs of electrostatic spinning. 10,000 V + direct current. Spinneret to ground spacing 50 mm. Solution feed rate 0.035 cc/min.

o.d. capillary. Both a change to negative polarity and an increase in o.d. to 2.4 mm had little effect on jet length, mean fiber diameter, or optimum feed rate.

Effect of Surrounding Gas. Some interesting results were obtained by surrounding the spinneret and grounded collector with air of different humidities, with helium, and with Freon®-12 (CCl_2F_2). The usual spinning atmosphere was air at 30% to 40% relative humidity. In dry air (<5% R.H.), the spinning drop tended to dry out, and spin-

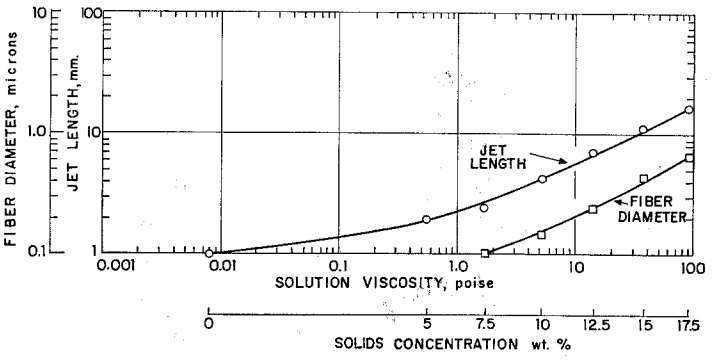

FIG. 3. Effect of viscosity on jet length and fiber diameter. 10,000 V + direct current. Spinneret to ground spacing 50 mm.

TABLE I

SOLIDS CONTENT OF FIBER

Fibers Spun from Acrylic Resin-Dimethyl Formamide Solutions. 10,000 Volts + D.C., 50 mm Spinneret to Ground Spacing. Humidity 47%.

Wt % Solid in DMF	Solution feed rate, (cc/min)	Polymer rate (g/min)	Wt % solid in fresh web	Wt % of DMF evaporated in spinning
10	0.035	0.0034	46.8	87.4
12.5	0.035	0.0042	28.0	63.2
12.5	0.087	0.0116	19.6	41.3

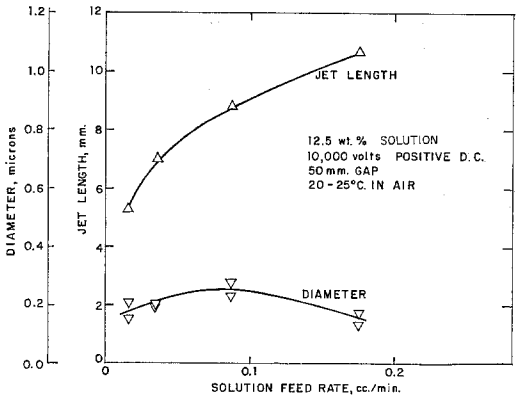

FIG. 4. Effect of feed rate on jet length and fiber diameter.

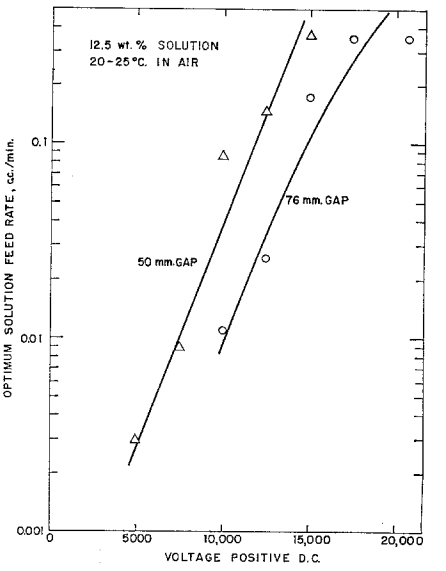

FIG. 5. Optimum feed rate as function of voltage and gap.

ning could be carried out for only 1 or 2 min. In humid air (>60% R.H.), the fiber from a 12.5% solution did not dry properly and tangled above the grounded screen. No spinning could be done in a helium atmosphere, because the gas started breaking down electrically at 2500 V. At 3000 V, corona current reached 40 μa, or about 100-fold that obtained in air at the same voltage.

Fibers spun in Freon®-12 gas were from 1.4 to 2.6 times the diameter of fibers spun in air at otherwise identical conditions. At 10,000 and 15,000 V positive (50- and 75-mm gap, respectively) small fiber offshoots from the main fiber were visible in the flash photographs. The fiber offshoots originated in the first few centimeters of the main fiber as measured from the end of the jet. About 20 could be counted in one photograph, and they all seemed to originate at, or be accompanied by, sharp bends in the main fiber.

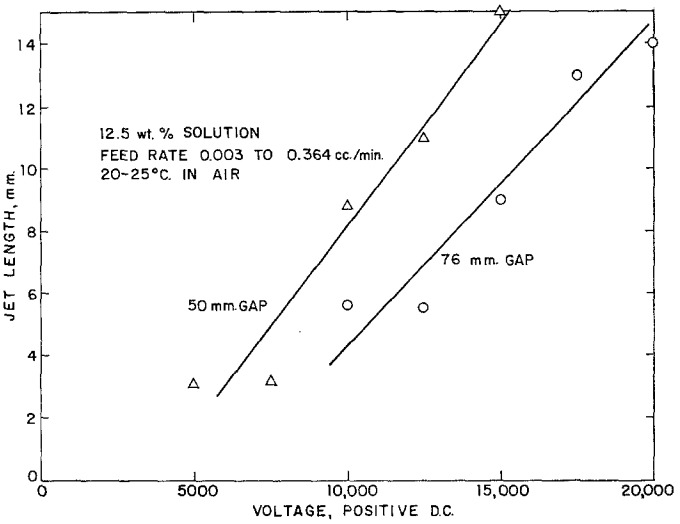

FIG. 6. Jet length at optimum feed rate.

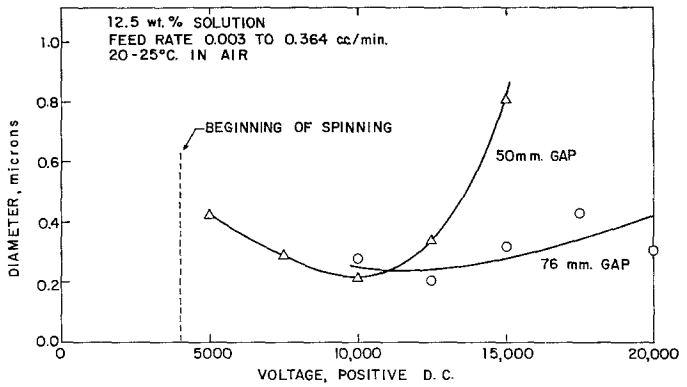

FIG. 7. Microfiber diameter at optimum feed rate from electron photomicrographs.

This behavior is probably due to the higher breakdown voltage of Freon®-12 as compared to air,[1] which would allow the fiber to retain its electric charge for a longer period of time. A 1-min exposure of a spinning fiber in air in a darkened room showed a corona glow for about 1 cm in the region below the spinning drop, indicating that the fiber remained charged for a finite length of time.

[2] 17,000 *vs.* 5000 V spark breakdown voltage at 1 atm for a point-plane geometry. The positive point electrode consisted of a tungsten wire (radius 0.025 cm) with hemispherical end. Gap was 0.3 cm.—H. C. Pollock and F. S. Cooper, *Phys. Rev.* **56**, 170 (1939).

DISCUSSION

The process of electrostatic spinning may be broken down into two parts: (1) the distortion of the spinning drop resulting in fluid dynamic instability, and (2) the continuous drawing of a fiber from a point on the drop. The first part of this mechanism has been analyzed in the literature. Hendricks *et al.* (6) calculated the minimum spraying potential of a suspended, hemispherical, conducting drop in air as

$$V = 300\sqrt{20\pi\gamma R}, \qquad [1]$$

where V is the voltage in volts, γ the surface tension in dynes/centimeter, and R the drop

radius in centimeters. Above this potential, the drop becomes fluid dynamically unstable, meaning that a slight disturbance of the surface will propagate itself. Hendricks' calculation method involved an energy balance between the potential energies of the electric charge and surface tension, and the kinetic energy of motion (using Legendre polynomials) of the pendant drop. For a liquid drop in air with $R = 0.1$ cm, $V = 6600$ V, in good agreement with experimental data on the acrylic resin-DMF system. If the surrounding medium is not air but a nonconducting liquid immiscible with the spinning fluid, drop distortion will be greater at any given electric field and, therefore, the minimum spinning voltage will be reduced (7).

Electric Field Map and Calculation of Jet Radius. The spinning process itself is best analyzed by means of an electric field map. Figure 8 shows maps for two possible cases based on approximate calculations (8). On the left of the center line, typical equipotential lines are sketched for a fully conducting jet, in which case the lines run parallel to the jet. This situation would hold for a liquid metal, and a downward accelerating force could exist only if the jet is interrupted and forms droplets. On the right of the center line, equipotential lines are drawn for a jet, which is electrically conducting above a hemispherical boundary with radius r_0, but nonconducting below it. Since the exact charge distribution below the boundary is not known, the equipotential lines are drawn as if the jet was not charged below the boundary. Since the linear charge density in the jet is likely to decrease with increasing distance from the boundary, the electric field in this region will not differ greatly from the one graphed. The overall effect of the electric field is a downward force on the charged jet which draws it into a continuous fiber.

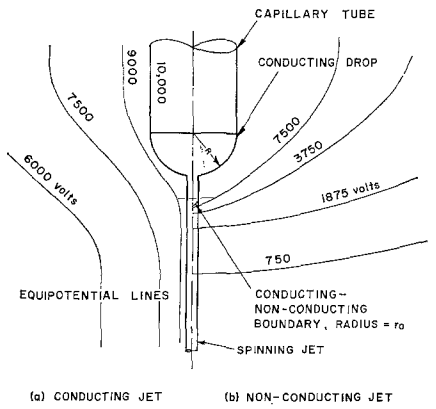

FIG. 8. Electrostatic field maps (schematic).

An interesting question concerns the magnitude of the radius r_0 in the "nonconducting" case and how it can be derived from basic considerations of the electric and flow phenomena. To solve for r_0, a simplified equation for charge density in the liquid jet is developed. The main assumption is that as each liquid element moves downward across the conducting/nonconducting boundary, the element temporarily retains the electric charge it had above the boundary. This charge may be related to the voltage of the conducting region by the equation expressing the charge/voltage relation for a spherical drop with radius r_0. This equation is (8)

$$q = 4\pi V \epsilon r_0 . \qquad [2]$$

Assume that as the liquid element flows downward, this charge becomes distributed over a liquid cylindrical element of radius and length r_0. Then the charge per unit mass of liquid becomes

$$\frac{q}{m} = \frac{4\pi\epsilon V r_0}{\rho\pi r_0^3} = \frac{4\epsilon V}{\rho r_0^2} \qquad [3]$$

and

$$I_{\text{transport}} = \frac{q}{m}\dot{m}_0 = \frac{4\epsilon V \dot{m}_0}{\rho r_0^2} . \qquad [4]$$

If the axial voltage gradient is given in units of V/r_0, the axial conduction current is

$$I_{\text{conduction}} = \pi r_0^2 \sigma \left(k_1 \frac{V}{r_0}\right), \qquad [5]$$

where k_1 is smaller than 1. Also let

$$I_{\text{transport}} = k_2 I_{\text{conduction}}$$

and since k_2 is a factor much greater than 1,

$$I_{\text{transport}} \sim I_{\text{total}} = I.$$

Combining these equations, we obtain

$$r_0 \sim \sqrt{4\epsilon V \dot{m}_0/\rho}; \quad [6]$$

$$k = \frac{4\epsilon \dot{m}_0}{\pi\sigma r_0^3 \rho} \sim \frac{I}{\pi\sigma V r_0}; \quad [7]$$

$$r_0 = \sqrt[3]{\frac{4\epsilon \dot{m}_0}{k\pi\sigma\rho}}. \quad [8]$$

Numerical values of r_0 and k can be calculated for typical spinning conditions. For V = 10,000 V, $I = 10^{-6}$ A, $\dot{m}_0/\rho$ = 0.00145 cc/sec, and $\sigma = 5 \times 10^{-5}$ A/V-cm for acrylic DMF solutions, r_0 = 16 μ and k = 0.00080. The value of r_0 so obtained compares with a collected fiber radius at laydown (not dry) of 0.31 μ and an observed radius at the tip of the spinning drop of 60 μ. Since the transition between the perfectly conducting and nonconducting regions of the jet may actually occur at some distance down from the drop, r_0 = 16 μ seems quite reasonable.

Effect of Electric Conductivity. Equation [8] indicates that the jet radius varies inversely as the cube root of electric conductivity. On the other hand, conductivity of various liquids covers a vast range. For mercury ($\sigma = 10^4$ A/V-cm) and liquid polyethylene ($\sigma = 10^{-16}$ A/V-cm) at the same flow rate and with k assumed constant, r_0 is calculated as 0.027 μ and 12.7 cm, respectively. In the former case, surface tension would dominate and only fine droplets would be sprayed off. In addition, the very high field strength would result in atmospheric breakdown. In the latter case, 12.7 cm is so large considering the usual spinning geometry that (1) the spinning drop, being appreciably larger than the jet, could no longer be suspended from a tube by surface tension, and (2) required voltages according to Eq. [1] would be of the order of 10^6 V. Alternately, flow rate $\dot{m}_0$ would have to be reduced manifold to compensate for the low value of σ.

Spinning Velocity. On the basis of the simple power balance

$$IV = \dot{m}_s v_s^2/2, \quad [9]$$

where $\dot{m}_s$ and v_s are the mass flow rate and spinning velocity of the wet fiber, spinning velocities were calculated to be 275 to 380 m/sec for experiments with 12.5% solution at voltages from 10,000 to 20,000 V and with the use of a 28% polymer concentration in the spinning fiber (see Table I) for calculation purposes. These velocities are close to the velocity of sound in air. Calculations of spinning velocity from material balances gave values of 970 to 7300 m/sec, but these are being discounted because of uncertainties inherent in estimating fiber diameter at laydown.

To calculate the rate of the electric drawdown from the point where the spinning jet becomes essentially nonconducting, we assume that all electric energy goes to kinetic energy, that the axial field intensity below the conducting/nonconducting boundary is equal to that of an electrically charged sphere of radius r_0, and that the volumetric charge density in the jet remains constant and unchanged from its value above the boundary. Then

$$E = Vr_0/y^2, \quad [10]$$

where y is the axial distance from the center of the hemisphere. Using Eq. [3] and neglecting the effect of viscosity, we obtain for the acceleration of the filament

$$a = \frac{F}{m} = E\frac{q}{m} = \frac{4\epsilon V^2}{\rho y^2 r_0}. \quad [11]$$

The boundary conditions are $v = 0$ and $y = r_0$ at $t = 0$.

Numerical solutions of [11] for fiber velocity and diameter are given in Fig. 9 and 10. Two cases are given, one where no solvent evaporates prior to the final velocity and the other where some solvent evaporates giving 28% solid concentration. The true drawdown should fall between these two cases. Evident from the figures is the very rapid change in velocity and diameter due to the

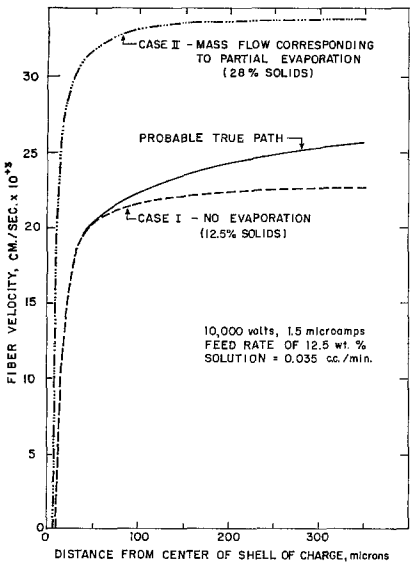

FIG. 9. Fiber velocity predicted from electric drawdown equation, Eq. [11].

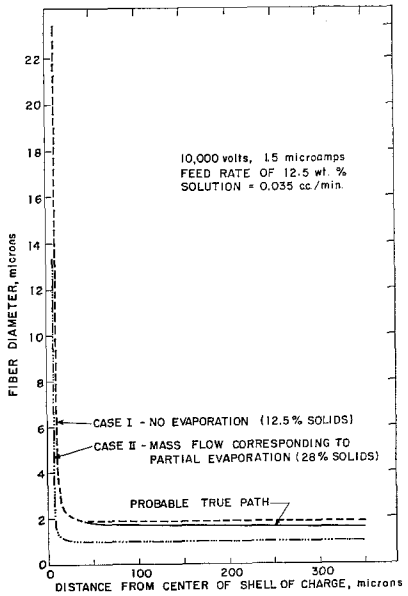

FIG. 10. Fiber diameter predicted from electric drawdown equation, Eq. [11].

electrical force. The initial acceleration was calculated to be 2.4×10^8 times gravity.

SUMMARY

Fibers from 0.05 to 1.1 μ in diameter were spun from polyacrylonitrile solutions by applying 5000 to 20,000 V direct current to small drops hanging from a metal capillary. Although the spinning process appears to the naked eye as a hazy cloud, microsecond flash pictures proved that only a single filament is spun at a time and that the filament forms many loops which fall to the electrical ground. The spinning velocity reached and perhaps exceeded the velocity of sound in air. Fiber diameter remained relatively constant over a tenfold range of flow rate but increased approximately as the 0.5 power of solution viscosity. The importance of the electical conductivity was shown by an electric field map. Estimates were made of the required jet radius for continuous spinning. If electric conductivity is too high, only droplets can be generated, whereas if the electric conductivity is too low, flow rates for sustained spinning might have to become extremely small for reasonable geometries. Calculations showed that drawdown is extremely rapid, maximum acceleration being of the order of 10^8 g's.

ACKNOWLEDGMENT

Several persons generously contributed advice and assistance in the development of the experimental program and theoretical treatment. Of these, I would like to mention chiefly F. S. Fountain, who developed techniques and did the initial work on electrostatic spinning of acrylic solutions, and W. O. Johnson, who suggested the photographic flash technique.

NOMENCLATURE AND TYPICAL DIMENSIONS

a = acceleration, cm/sec^2.
E = electric field intensity, volts/cm.
F = force, dynes.
I = current, amp.
k = k_1k_2, dimensionless.
k_1 = axial voltage gradient in jet in units of V/r_0.
k_2 = $I_{\text{transport}}/I_{\text{conduction}}$.
m = mass of a volumetric element of the jet, gm
$\dot{m}$ = mass flow rate, gm/sec.
q = electric charge, coulombs.
r = jet or filament radius, cm.
R = drop radius, cm.
t = time, sec.

v = velocity, cm/sec.
V = voltage, volts.
y = axial distance, cm.
γ = surface tension, dynes/cm.
ϵ = permittivity, farads/cm = coulombs/volt-cm.
ϵ_0 = permittivity of free space, 8.85×10^{-14} farads/cm = 10^{-7} gm-cm/volts^2-sec^2.
ρ = density, gm/cc.
σ = electric conductivity, mhos/cm or amp/volt-cm.

Subscripts

o = initial; feed solution.
s = filament just after being spun.

REFERENCES

1. DROZIN, V. G., *J. Colloid Sci.* **10,** 158 (1955).
2. VONNEGUT, B., AND NEUBAUER, R. L., *J. Colloid Sci.* **7,** 616 (1952).
3. ZELENY, J., *Proc. Cambridge Phil. Soc.* **18,** 71 (1916); *Phys. Rev.* **10,** 1 (1917); *J. Franklin Inst.* **219,** 659 (1935).
4. FORMHALS, A., U. S. Patents 1,975,504, 2,077,373, 2,109,333, 2,116,942, 2,123,992, 2,158,415, 2,158,416, 2,160,962, 2,187,306, 2,323,025, and 2,349,950.
5. GLADDING, E. K., U. S. Patent 2,168,027.
6. HENDRICKS, C. D., JR., CARSON, R. S., HOGAN, J. J. AND SCHNEIDER, J. M. *AIAA Journal* **2,** 733 (1964).
7. O'KONSKI, C. T., AND THACHER, H. C., JR., *J. Phys. Chem.* **57,** 955 (1953).
8. KRAUS, JOHN D., "Electromagnetics," Chapters 1 and 2. McGraw-Hill, New York, 1953.